



Island divertor experiments on the Wendelstein 7-AS stellarator

K. McCormick^{*}, P. Grigull, R. Burhenn, R. Brakel, H. Ehmler, Y. Feng, R. Fischer, F. Gadelmeier, L. Giannone, D. Hildebrandt, M. Hirsch, E. Holzhauser, R. Jaenicke, J. Kisslinger, T. Klinger, S. Klose, J.P. Knauer, R. König, G. Kühner, H.P. Laqua, D. Naujoks, H. Niedermeyer, E. Pasch, N. Ramasubramanian, N. Rust, F. Sardei, F. Wagner, A. Weller, U. Wenzel, A. Werner

Max-Planck-Institut für Plasmaphysik, Boltzmannstrasse 2, EURATOM Ass., 85748 Garching bei Munchen, Germany

Abstract

A promising new operational regime on the Wendelstein stellarator W7-AS has been discovered, fulfilling the conditions of optimal core behavior in combination with edge parameters suitable for successful divertor scenarios. This regime, the high density H-mode (HDH), displays no systematically evident mode activity, and is edge localized mode (ELM)-free. It is extant above a power-dependent threshold density and characterized by flat density profiles, high energy- and low impurity-confinement times and edge-localized radiation. Impurity accumulation, normally associated with ELM-free H-modes, is avoided. Quasi-stationary discharges with line-averaged densities \bar{n}_e to $4 \times 10^{20} \text{ m}^{-3}$, radiation levels to 90%, and partial plasma detachment at the divertor target plates can be simultaneously realized. Energy confinement is up to twice that predicted by a conventional scaling. HDH has been attained for both H^+ and D^+ plasmas. The development of plasma energy as a function of density shows an isotopic dependence.

© 2003 Elsevier Science B.V. All rights reserved.

PACS: 52.55.Hc

Keywords: Stellarator; W7-AS; Island divertor; H-mode; Impurity control; Plasma properties

1. Introduction

The island divertor concept is an implicit element of the Wendelstein stellarator line of development. However, in contrast to the extensive experience with poloidal field divertors for tokamaks, related research on stellarators is in its absolute infancy. This paper reports on advances associated with the first-ever realization of the island divertor on W7-AS ($R = 2 \text{ m}$, $a_{\text{eff}} \leq 0.16 \text{ m}$, $B_t \leq 2.5 \text{ T}$), which is similar in major aspects to that of

the W7-X stellarator ($R = 5.5 \text{ m}$, $a_{\text{eff}} \sim 0.5 \text{ m}$) now under construction in Greifswald [1]. In particular, an exciting new confinement regime exhibiting high energy τ_E - and low impurity τ_{imp} -confinement has been discovered, termed the high density H-mode (HDH) [2]. These properties enable very high line-averaged densities \bar{n}_e (up to $4 \times 10^{20} \text{ m}^{-3}$) to be attained under controlled, quasi-stationary conditions with separatrix densities (up to $8 \times 10^{19} \text{ m}^{-3}$) and fractional radiation levels (up to 90%) easily permitting access to divertor detachment scenarios. Thus a database of edge/SOL/divertor experience is being compiled which serves as reference material for validation of the 3D edge transport code EMC3/EIRENE [3].

W7-AS is a modular, low-shear stellarator with five magnetic field periods. Over one period the plasma

^{*} Corresponding author. Tel.: +49-89 3299 1932; fax: +49-89 3299 2584.

E-mail address: gkm@ipp.mpg.de (K. McCormick).

shape varies from a standing ellipse ($\phi = 36^\circ$) to a triangle ($\phi = 0^\circ$) and back again. Depending on the rotational transform τ_a the plasma is bounded either by smooth flux surfaces or by a separatrix formed from naturally occurring magnetic islands (at edge iota values $\tau_a = 5/m$ with $m = 8, 9, 10, \dots$). Control coils act to enhance or reduce the radial extent of the edge islands, thereby altering the plasma radius as well as influencing the field line pitch inside the islands [4,5]. The five (top–bottom) divertor module pairs, installed summer 2000, provide an all-graphite plasma-target interaction region for the first time in W7-AS and are optimized for $\tau_a = 5/9$, but function as well for $\tau_a = 5/8$ or $5/10$. (The vessel walls are of stainless steel.) The modules have a length of about 700 mm, covering only about 25% of the toroidal circumference. Hence, in contrast to a tokamak poloidal divertor, the island divertor concept entails the use of discrete elements – creating a very 3D edge environment, thereby enhancing the demands placed on edge/divertor diagnostics. For particle control, titanium gettering behind the inner baffle region has been prepared. It has not yet been activated – beyond preliminary tests – nor even found to be necessary for the HDH investigations. Since divertor-relevant situations exploit densities considerably in excess of 10^{20} m^{-3} , neutral beam injection (NBI) heating is the mainstay of the program (the electron cyclotron resonance heating (ECRH) cutoff density is $1.2 \times 10^{20} \text{ m}^{-3}$), with a nominal injected power of up to $P_{\text{nbi}} = 4 \text{ MW}$ ($P_{\text{abs}} \sim 2.8 \text{ MW}$ absorbed). Over the past year most operational experience has been with $\text{H}^0 \rightarrow \text{H}^+$ plasmas. Results from a recent $\text{D}^0 \rightarrow \text{D}^+$ campaign are reported here for the first time. Further details relating to the plasma-target interaction region are covered in companion papers with respect to experimental observations [6,7] and edge-code interpretation [8]. A survey of edge/divertor-related diagnostics is given in [9].

2. Experiments

On W7-AS in the past, it has been impossible under limiter conditions to produce high-power, high-density, quasi-stationary NBI discharges with edge densities adequate for acceptable plasma–wall interaction scenarios [4,10]. Since τ_E and τ_{particle} as well as τ_{imp} increase with density [11,12], such discharges tended to evince impurity accumulation, lack of density control and subsequent radiation collapse [13]. Note that here the emphasis is on ‘high performance’ discharges designed to produce separatrix densities n_{es} large enough to drive divertor detachment, or to probe β -limits at low B_t . Within the operational limits of W7-AS there are no essential difficulties with ECRH discharges, or with NBI at the $P_{\text{nbi}} = 0.5 \text{ MW}$ level, for example.

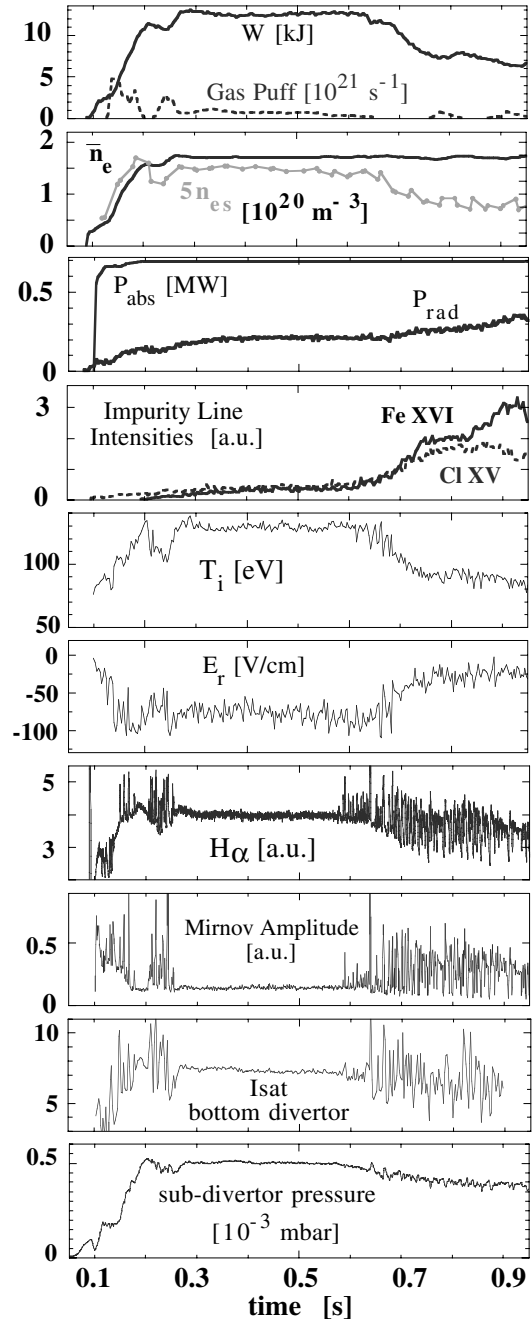


Fig. 1. A discharge displaying a spontaneous transition from HDH (~ 0.28 – 0.62 s) to NC ($> 0.65 \text{ s}$) because $\bar{n}_e < \bar{n}_e^{\text{thr}}$. Time traces of stored energy W , gas puff rate, line-averaged density \bar{n}_e , separatrix density n_{es} , absorbed NBI power P_{abs} , total radiated power P_{rad} , impurity line intensities, ion temperature in the steep gradient region (for HDH) and electric field at same point, global H_α intensity over a divertor module, amplitude for a Mirnov coil, saturation current to all target plate probes on the bottom divertor, and the lower sub-divertor neutral pressure. $\delta x \sim 3.8 \text{ cm}$, $B_t = -2.5 \text{ T}$, $P_{\text{nbi}} = 1 \text{ MW}$, $\text{H}^0 \rightarrow \text{H}^+$. The NBI fueling rate is $\sim 10^{20} \text{ s}^{-1}$.

2.1. Characteristics of normal confinement and HDH

The HDH regime is accessible only via NBI ($P_{\text{nbi}} \geq 1$ MW) since the transition density threshold \bar{n}_e^{thr} lies above the cutoff density ($1.2 \times 10^{20} \text{ m}^{-3}$) for the conventional 140 GHz ECRH system (second harmonic X-mode). Fig. 1 displays the temporal evolution of core/edge/divertor-plasma quantities for a $P_{\text{nbi}} = 1$ MW discharge in hydrogen where $\bar{n}_e \sim 1.6 \times 10^{20} \text{ m}^{-3}$ is very slightly below \bar{n}_e^{thr} . At the 1 MW level such discharges at the outset tend to attain HDH and then fall back into normal confinement (NC) as time proceeds, consequently permitting a contrasting study of NC-HDH under almost identical setup conditions. This transient achievement of HDH is probably related to the strong external gas puff initially necessary to effect the rapid density increase, basically forcing HDH-like n_e -profiles (see below) through enhanced edge fueling. Later, the inherent neutral recycling at the edge is not adequate to sustain the situation, leading to a relaxation of the n_e -profile into the NC-state. In any case, a strong gas puff concurrent with initiation of NBI, i.e. a rapid ramp-up of density, is essential for controlled, reliable entrance into HDH. (However, principally, HDH may also be reached by hard puffing in a fully developed NC discharge [14].)

In Fig. 1 the cardinal elements of HDH are seen over the time span $\sim 0.28\text{--}0.62$ s: a higher stored energy W and lower plasma radiation P_{rad} – whereby the faster attainment of stationarity of $W(t)$ in comparison to $P_{\text{rad}}(t)$ presumably reflects the impurity redistribution time. The access phase into HDH is accompanied by edge localized mode (ELM) activity – registered as H_x -bursts as well as Mirnov coil activity, which then subsequently diminishes to a much lower level. This, in addition to the sheared poloidal plasma flow and associated electric field E_r is characteristic of entrance into an ELM-free H-mode (H*) on W7-AS [15,16]. The extraordinary difference is the total lack of concomitant peaking of radiation and subsequent radiation collapse, which normally materializes in an H*-phase. This is underlined in Fig. 1 by the low level and constancy of impurity line radiation in HDH, in opposition to the following rapid increase during the NC-phase. The radial change in impurity transport is clearly illustrated by radiation profiles $P_{\text{rad}}(r)$ measured by a bolometer array (Fig. 2): For HDH, $P_{\text{rad}}(r)$ is stationary and concentrated at the extreme edge, whereas the NC-phase shows peaked $P_{\text{rad}}(r)$ increasing in time. Another important aspect of HDH is the higher n_{es} , which leads to increased particle flux to the target plates (in Fig. 1, registered by an increase in I_{sat} to the Langmuir probes and the higher level of H_x), and therefore higher subdivertor neutral pressure [17]. This is important for active pumping scenarios. A high n_{es} is also a primary prerequisite for the attainment of detached plasmas.

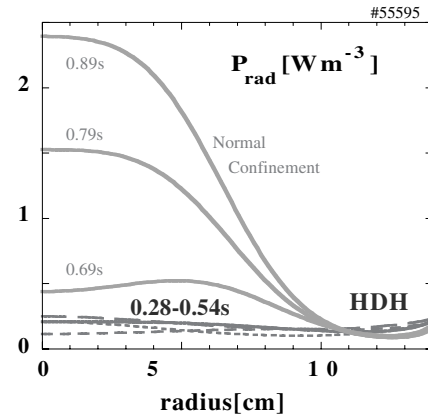


Fig. 2. Radiation profiles from a bolometer array at various time points in the HDH- and NC-phases of the discharge of Fig. 1.

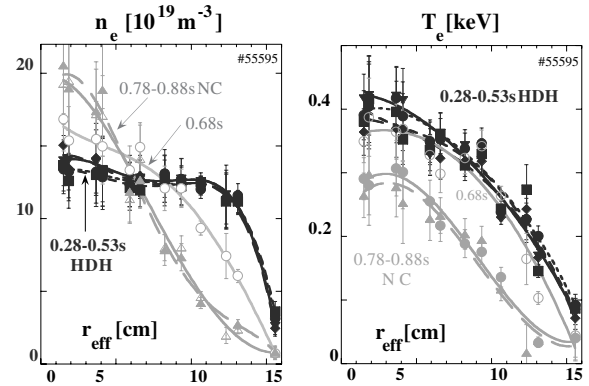


Fig. 3. Density and temperature profiles at various time points in the HDH- and NC-phases of discharge #55595. The fitted curves are polynomials to guide the eye. They do not accurately reflect profiles at the very edge. The outermost point lies within a magnetic island.

Attendant to HDH is a dramatic flattening of the n_e -profile with a sharp gradient at the edge. Fig. 3 juxtaposes n_e - and T_e -profiles for HDH- and NC-phases of the discharge of Fig. 1. $T_e(r)$ is enhanced, and shows a tendency towards a slight T_e -pedestal, but otherwise is not substantially altered in shape. This formation of an edge transport barrier in density, with rather parabolic T_e -profiles, is also characteristic of H* – albeit, largely documented at $P_{\text{nbi}} \sim 0.5$ MW [16]. An edge dedicated Thomson scattering system (radial resolution $\delta r \sim 4$ mm) resolves the steep HDH pressure gradient profile (Fig. 4), which cannot be satisfactorily registered by the 20 Hz YAG system ($\delta r \sim 1.5$ cm). There is considerable uncertainty as to the correctness of the r_{eff} scale in Figs. 3 and 4. Due to the large islands associated with this particular configuration, it has not yet been possible to

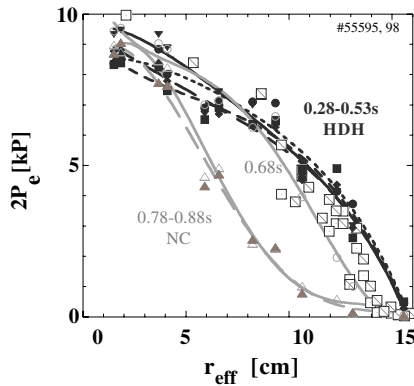


Fig. 4. Electron pressure profiles: Derived from the n_e - and T_e -values of Fig. 3, again with only guiding fits, and also from the edge/central Ruby Thomson scattering system which resolves the steep gradient region (square, open symbols; no fit).

produce a magnetic field equilibrium for finite β . (In #55595, the maximum plasma energy of ~ 13 kJ corresponds to $\langle \beta \rangle \sim 0.6\%$.) – which, however, is particularly critical for correct placing of the outermost YAG points. Such will not influence the form of the profiles in a crucial fashion, but apparently makes the plasma radius appear larger than the 12 cm of the vacuum field configuration. Preliminary calculations with the equilibrium code HINT [18] for a related configuration generically indicate the plasma radius should not markedly change with β [19]. Notwithstanding, these considerations are not relevant for the edge system, so the gradient is correctly resolved (here, the relative position is adjusted to fit YAG). Finally, in passing it is interesting to note that the pressure profiles for NC are very peaked and it under such conditions that ELMing/dithering in NC takes place as the transition threshold is approached – whereas the ELM-free situation of HDH is characterized by a steep pressure gradient at the edge.

Study of the spatiotemporal behavior of highly ionized states of laser-ablated aluminum provides an indication of impurity transport over the core region [2]. At $P_{\text{nbi}} = 2$ MW, it is found the NC regime can be characterized by an impurity diffusion coefficient $D \sim 0.085 \pm 0.015$ m²/s and an inwards convective velocity $v \sim -10(r/a_{\text{eff}})$ m/s. The HDH regime yields $D \sim 0.095 \pm 0.015$ m²/s and $v \sim -(2.7 \pm 0.8)(r/a_{\text{eff}})$ m/s, i.e. $D(\text{HDH}) \sim D(\text{NC})$, but $v(\text{HDH}) < v(\text{NC})$. The NC-values for D and v are similar to those found for NBI-heated plasmas previously investigated on W7-AS [20]. They are also comparable to the v/D ratio found on tokamaks in ELM-free H-mode phases [21]. Thus within the framework of this Ansatz, during HDH the reduced inwards pinch evidently causes diffusion to dominate over convection, leading to an absence of impurity peaking. Earlier studies on W7-AS have shown background ions to display similar confinement behavior to

impurities in terms of D [22]. In the present study, the flat n_e -profiles, as well as the realization of density control in HDH are at least congruous with H⁺ transport being related to that of impurities, but the evidence is not conclusive. Definitive statements about transport in the steep n_e -gradient region are not yet possible.

Attainment of HDH also affects the interaction pattern at the target plates: Fig. 5 shows a lower target plate (in the light of H_z) in the NC phase, and Langmuir probe I_{sat} profiles across the target plate at the indicated positions for NC and HDH. The $I_{\text{sat}}(\text{NC})$ distribution corresponds closely to that expected for the given edge

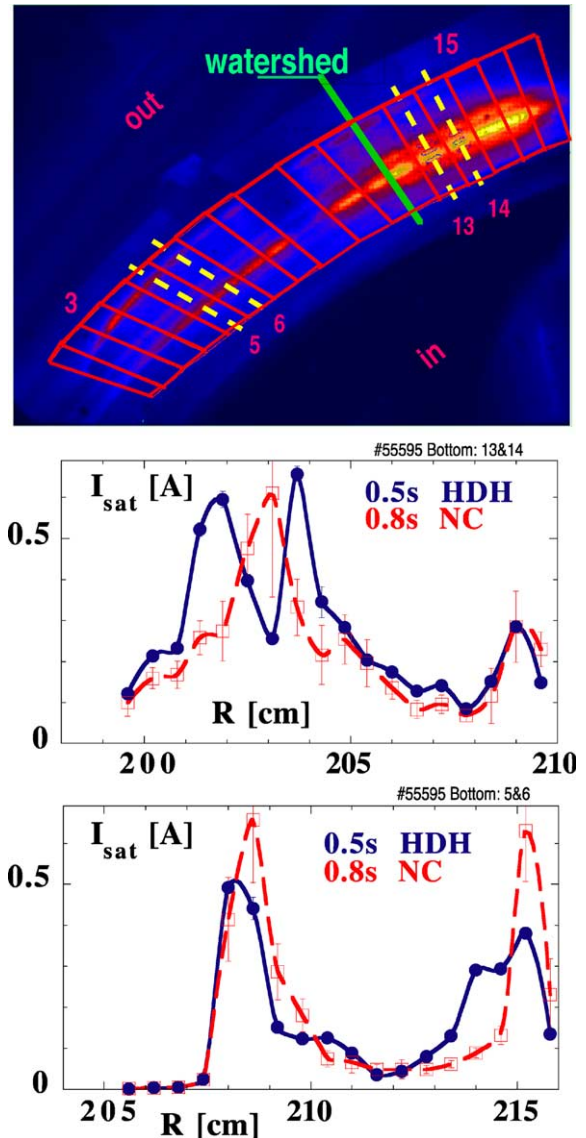


Fig. 5. Lower divertor target: In the light of H_z during the NC-phase of #55595 (top figure). I_{sat} current profiles of Langmuir probe arrays in tiles 13–14 (middle) and 5–6 (bottom).

island configuration. Nonetheless, the ‘splitting’ of the interaction zone around $R \sim 203$ cm into two peaks for tiles 13–14 during HDH, while entirely typical, is not yet understood. There are also up-down asymmetries in deposition patterns (not shown), where EMC3/EIRENE can offer the explanation of $E \times B$ drifts within the island structure [6,8]. These pictures serve to illustrate the complex nature of the plasma-target interaction region, and the necessity of a close coupling between experiments and modeling in order to promote even basic understanding. More experimental details are contained in [6].

Fig. 6 summarizes the behavior of the energy confinement time $\tau_E = W/P_{\text{abs}}$ and dwell time τ_{Al} of laser-ablated aluminum obtained from \bar{n}_e -, P_{nbi} -scans for quasi-stationary discharges of duration ≥ 0.5 s as a function of the line-averaged density \bar{n}_e for both hydrogen and deuterium plasmas. The apparent jumps of τ_E at $\bar{n}_e \sim 1.5$ and $1.8 \times 10^{20} \text{ m}^{-3}$ for hydrogen (for $P_{\text{nbi}} = 1$ and 2 MW, respectively) mark the threshold densities \bar{n}_e^{thr} for transition into HDH at each power level. τ_E -values in NC follow the scaling $\tau_E^{\text{ISS95}} = 0.26 t_a^{0.4} B_t^{0.83} a^{2.21} R^{0.65} \bar{n}_e^{-0.51} P_{\text{abs}}^{-0.59}$ [11], whereas for HDH(H^+) one finds $\tau_E \sim 2\tau_E^{\text{ISS95}}$, except during detachment where P_{rad} profiles begin to encroach into the core plasma (cf. Fig. 9). In contrast, deuterium discharges do not exhibit a discontinuous change in confinement. Rather, $\tau_E(\text{D}^+)$ is almost linear with \bar{n}_e , and for $P_{\text{nbi}} = 2$ MW continues to increase at densities where $\tau_E(\text{H}^+)$ has saturated. From the profiles of Fig. 7 this behavior derives from the density pedestal which develops in the NC-phase for deuterium, along with initially lower T_e -values upon entrance into HDH. Detachment (solid symbols in Fig. 6) ensues at higher densities. Nonetheless, $\tau_{\text{Al}}(\text{D}^+)$ decreases with density, reaching similar values as $\tau_{\text{Al}}(\text{H}^+)$, so the important HDH feature of mitigation in τ_{imp} with the increase in τ_E is preserved. τ_E for deuterium is possibly higher than depicted in Fig. 6. Until precise calculations are available, which again requires an equilibrium, it is assumed the absorbed power is the same for both isotopes, even though the birth profiles for D^+ ions are much closer to the edge at higher densities.

In Fig. 6, the fractional radiated power $P_{\text{rad}}/P_{\text{abs}}$ grows smoothly with \bar{n}_e until $P_{\text{rad}}/P_{\text{abs}} \sim 0.5$, when higher values associated with the appearance of asymmetric edge radiation materialize (Fig. 9), leading to onset of partial plasma detachment at the target plates. Deuterium plasmas partially detach at the lower target plates for $P_{\text{rad}}/P_{\text{abs}} > 60\%$, and at both upper and lower plates for still higher radiation levels. There is also an isotope effect in n_{es} , which shows a jump at the NC \rightarrow HDH transition point for H^+ , but a continuous increase for D^+ . $n_{\text{es}}(\text{D}^+, \text{H}^+)$ attains maximum values $n_{\text{es}}^{\text{max}} \sim 3/4\text{--}6 \times 10^{19} \text{ m}^{-3}$ (for $P_{\text{nbi}} = 1\text{--}2$ MW) before dropping (2 MW, H^+ only) at partial detachment. τ_E mirrors the general behavior of n_{es} for both isotopes,

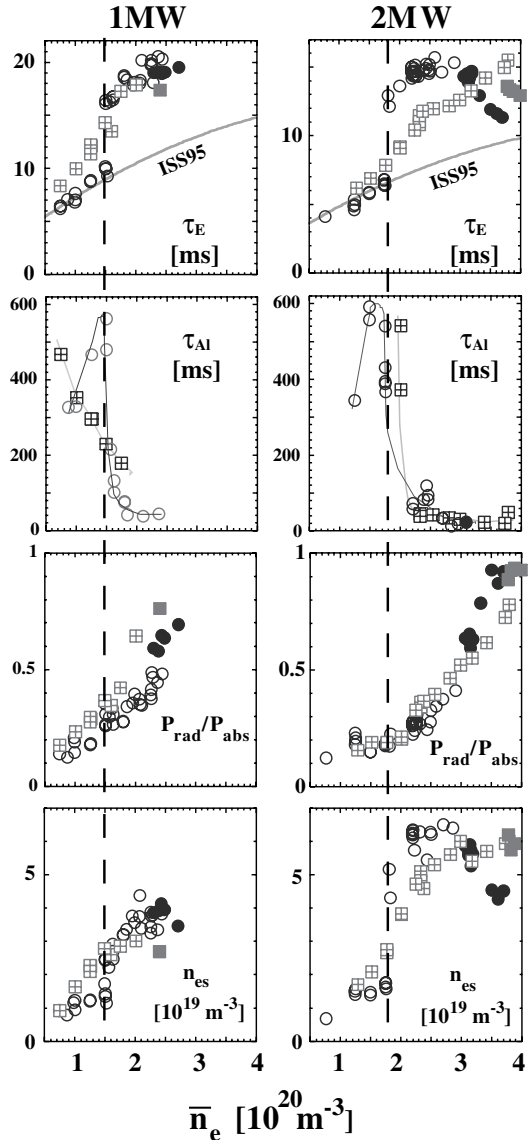


Fig. 6. $P_{\text{nbi}} = 1$ MW (left) 2MW (right). Comparison between $\text{H}^0 \rightarrow \text{H}^+$ (circles) and $\text{D}^0 \rightarrow \text{D}^+$ (crossed squares) quasi-stationary discharges. Full symbols denote partially detached conditions. Energy confinement time τ_E , exponential decay time τ_{Al} of laser ablated Al, radiated power fraction $P_{\text{rad}}/P_{\text{abs}}$ and separatrix density n_{es} . The dashed lines mark the NC-HDH boundary for hydrogen discharges. The τ_E^{ISS95} scaling is indicated. $\delta x \sim 3.8$ cm, $B_t = 2.5$ T.

denoting the significance of n_e profile forms in the determination of energy confinement.

The nature of isotopic trends for τ_E and n_{es} seen in Fig. 6 is clarified by the n_e - and T_e -profiles for a representative set of $P_{\text{nbi}} = 2$ MW discharges (Fig. 7), where the H^+ and D^+ examples span about the same line-averaged density. The deuterium density profile changes

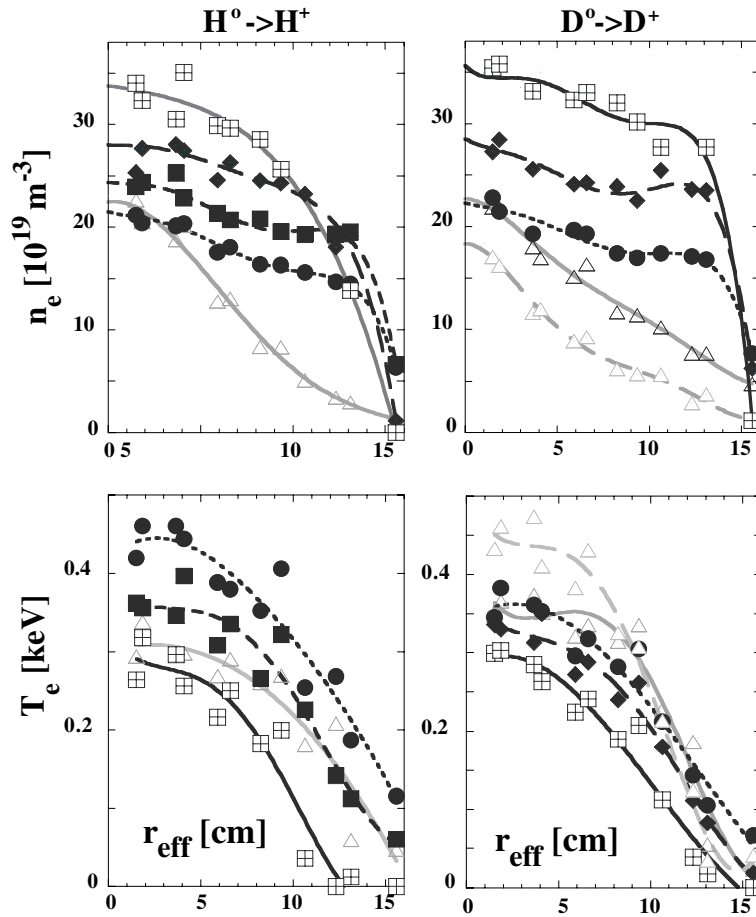


Fig. 7. n_e - and T_e -profiles for a \bar{n}_e -scan in hydrogen and deuterium plasmas. NC = open symbols, HDH = full symbols, crossed squares = partial detachment in HDH. $\delta x \sim 3.8$ cm, $B_t = -2.5$ T, $P_{\text{nbj}} = 2$ MW. #55561, 63–65, 69 (left); #55230, 37, 41, 46, 54 (right).

somewhat more continuously with \bar{n}_e , showing a smaller jump from NC to HDH when the profile becomes flatter. But, $n_e(r)$ for deuterium does not decrease at the edge when entering detachment, which accounts for the higher n_{es} and τ_E . In contrast, the lack of an enhancement in $T_e(r)$ at the deuterium transition to HDH contributes to a lower τ_E initially in comparison to hydrogen – but T_e at the edge does not decrease so much for deuterium during detachment. These higher n_{es} and T_{es} lead to $P_{\text{rad}}(r)$ profiles displaced further outwards for deuterium (not shown), also supporting the larger $\tau_E(\text{D}^+)$ at high \bar{n}_e . Presently, it is not clear if these effects are related simply to the different power and particle deposition profiles, or if they reflect a more fundamental isotopic transport dependence.

2.2. SOL/divertor plasma behavior

Fig. 8 shows the variation of peak power deposition, as measured by an IR camera, on target tiles #3 and #15

(see Fig. 5) for a density scan at $P_{\text{nbj}} = 2$ MW. One end of the divertor (#15) exhibits a strong decrease in power loading already before partial detachment, and continues to decrease moderately thereafter. Generally, tile #3 experiences less of an unloading. The particle flux measured by Langmuir probes in nearby tiles behaves similarly. The behavior of upstream temperature at the separatrix T_{es} , the downstream values T_{ed} as well as n_{es} and n_{ed} are considered in [6,8]. Of note is that the Langmuir probes find $n_{\text{ed}} \leq n_{\text{es}}$ over the entire operational range, meaning that partial detachment is attained without going through the high-recycling regime typical for tokamaks.

All of these phenomena are generally predicted by the 3D edge modeling code EMC3/EIRENE [3,8,23], i.e. the lack of a high-recycling regime, the drop of fluxes to the target plate already at moderate densities, and the toroidal distribution of power/particle deposition patterns for attached/detached situations. The behavior of neutral gas pressure in the subdivertor regions of up-down divertor modules as shown in Fig. 8, i.e. the strong

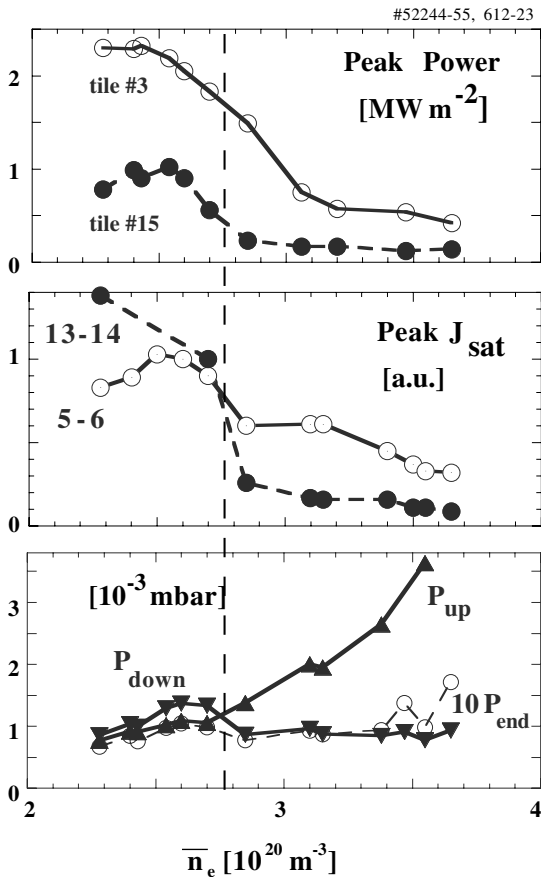


Fig. 8. Peak power to target plate tiles #3 and #15, from IR thermography for a density scan. Peak saturation current to Langmuir probes in tiles 5–6 and 13–14. Equivalent neutral gas pressures in the subdivertor of an upper (P_{up}) and lower (P_{down}) subdivertor module, and at the end of the lower module (P_{end} – multiplied by 10). The dashed line demarks the beginning of partial detachment. $\delta x \sim 3.3$ cm, $B_t = -2.5$ T. $P_{\text{nbi}} = 2$ MW, $\text{H}^0 \rightarrow \text{H}^+$.

asymmetry of $P_{\text{up}}/P_{\text{down}}$ in detachment, is not understood. However, the reproducibility of this phenomenon is such that it serves as a reliable ‘detachment indicator’, without having to consult the Langmuir probes. Considering Fig. 8, it is not surprising that a pressure drop ensues during detachment (lower divertor) since a detached plasma is expected to provide less baffling of subdivertor neutrals, and densities are never very high in the divertor region anyway. The increase in P_{up} must indicate the presence of an enhanced neutral source in the upper divertor. This is correlated with the appearance of an asymmetry in P_{rad} at detachment (Fig. 9). (Ultimately, it is the appearance of the asymmetry and the increase in P_{rad} which leads to a reduction of power flow to the target plates, driving the plasma into partial detachment.) Measurements of Balmer-line broadening

by a spectrometer viewing the upper divertor suggest the existence of a high-density, low temperature region in front of the target plate [24]. H_α/H_γ measurements additionally support the presence of a ‘density condensation’, i.e. a recombining region in the upper divertor [7]. Field reversal leads to a reversal of the up-down asymmetry (as well as of typical deposition patterns at the plates [6]), indicating a robust, physics-based phenomenon. In any case, the divertor pressures attained are predicted to be more than adequate for effective neutral pumping by Ti-gettering should it be activated. Finally, Fig. 8 illustrates that neutral compression (ratio of subdivertor to main chamber pressure) never attains large values, e.g. ~ 10 when the lower divertor is taken as reference. Nevertheless, attainment of H-mode-like plasmas appears not impaired by the high neutral pressure of $\sim 10^{-4}$ mbar near the wall.

All discussion thus far has concentrated on discharges where the x-point distance to the target plate was about 33–38 mm (Figs. 8, 9, 1–7, respectively). Nonetheless, detachment behavior is universal in nature with respect to diverted discharges as long as the distance δx between the separatrix and target plates (adjusted via control coils) is greater than about 2.4 cm for an upstream-downstream connection length of 100 m [6]. Nonetheless, for $0 \leq \delta x < 2.4$ cm the HDH-regime can also be established, albeit with the caveat that at high \bar{n}_e an oscillatory radiation collapse replaces controlled detachment. HDH is even accessible for a limiter plasma with $\delta x < 0$, but a high power level (3.5 MW) is necessary to avoid radiation collapse while building the density to the point where HDH is established.

3. Discussion and summary

For separatrix-bounded plasmas, the path to HDH at the beginning of the discharge (and also the back-transition, if present) is often accompanied by H-mode artifacts. In particular, the buildup of an edge-localized transport barrier is evident as well as its intermittent breakdown, manifested in ELMs. HDH itself is absolutely ELM-free. The HDH regime exhibits global similarities with the enhanced D_α H-mode (EDA) found on the Alcator C-Mod tokamak (primarily: ELM-free quasi-stationarity with no impurity accumulation) [25]. Other aspects do not appear to have a parallel: On W7-AS there exists a minimum threshold density, which increases with power, for example. Further, a key feature of the EDA H-mode is the presence of a quasi-coherent electromagnetic mode localized in the density pedestal region ($k_\theta \sim 5$ cm $^{-1}$, $f \sim 100$ kHz), which is found responsible for enhanced particle transport – leading to concomitant impurity flushing [25,26]. On W7-AS, a dedicated k-scan with a microwave relectrometer (78 GHz) covering $k_\theta \sim 0$ –10 cm $^{-1}$ over a

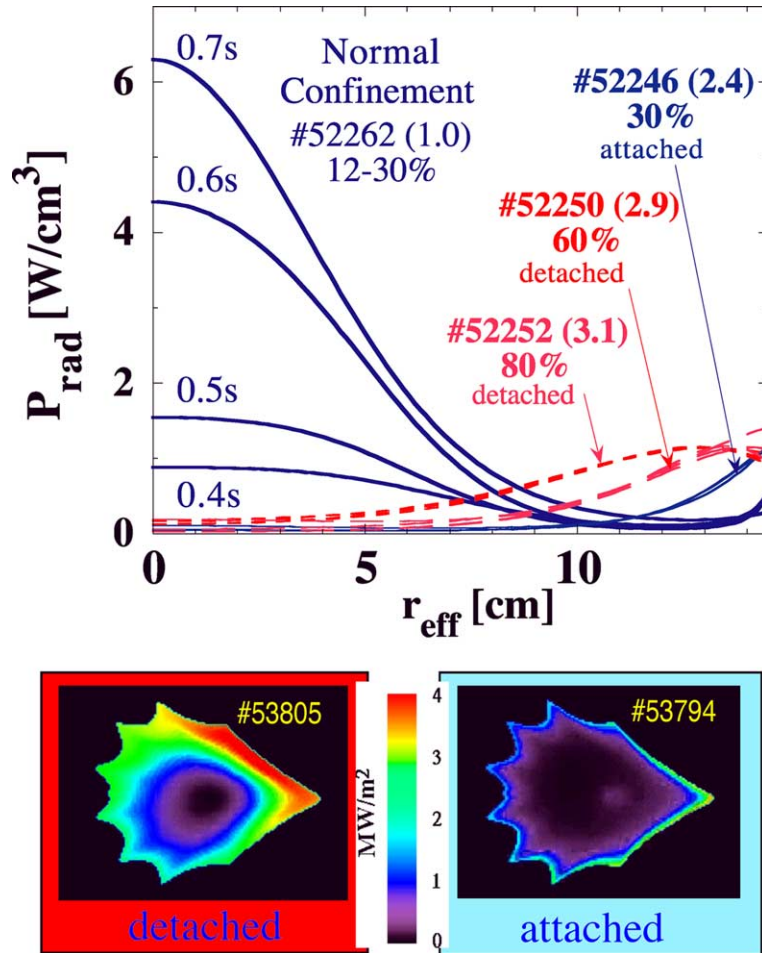


Fig. 9. Top: $P_{\text{rad}}(r)$ profiles from a bolometer array for discharges of Fig. 8. One NC-discharge and three HDH-discharges are depicted at four time points each over 0.4–0.7 s. \bar{n}_e (10^{20} m^{-3}) is given in parenthesis, followed by the fractional radiated power $P_{\text{rad}}/P_{\text{abs}}$. Bottom: Tomographic reconstruction of $P_{\text{rad}}(r)$ for $P_{\text{nbi}} = 2$ MW detached (#53805, $\bar{n}_e \sim 3.6 \times 10^{20} \text{ m}^{-3}$, $P_{\text{rad}}/P_{\text{abs}} \sim 90\%$) and attached cases (#53794, $2.5 \times 10^{20} \text{ m}^{-3}$, 27%).

frequency range 5–250 kHz for discharges of the type illustrated in Figs. 1–4 did not detect any mode activity. The cutoff density of $\sim 6 \times 10^{19} \text{ m}^{-3}$ placed the reflecting layer in the density gradient region inside the separatrix. Measurements at other frequencies, corresponding to cutoff densities of ~ 8 and $12 \times 10^{19} \text{ m}^{-3}$ have yielded similar results [27]. First tests of a scannable Mirnov coil designed to transiently probe the plasma edge, as on C-Mod [25], also have not revealed any systematic mode activity [28]. On the other hand, a common feature is some overlap of the edge T_e - and n_e -ranges and the associated collisionality ν^* [29,30]. On W7-AS $\nu^*(\text{H}^+)$ is typically around 0.2–0.3 in the plasma center, i.e. marginally collisionless. However, H^+ is collisional at the edge, and impurities are highly collisional over the entire cross section. This may turn out to be of principle importance for the understanding of HDH.

Partly due to the scaling of \bar{n}_e^{thr} with power, it has not been possible to substantially alter ν^* by augmenting P_{nbi} . The increase in \bar{n}_e^{thr} with P_{nbi} might be related to collisionality. However, the necessity to sharply increase the density in order to access HDH may also suggest the need to strike a balance between central fueling via NBI and edge density buildup by gas puffing and neutral recycling in order to produce flat n_e -profiles. Thus, higher P_{nbi} implies higher central fueling, which must be counteracted by higher gas puff rates, resulting in a higher \bar{n}_e^{thr} . Still another connection may play a role between the operational space of HDH and heating power level: On W7-AS the \bar{n}_e -threshold for attainment of the H-mode increases with power [4,10,16] (exactly vice-versa to the tokamak situation where an increase in density leads to an increase in the H-mode power threshold). If HDH requires H-mode like conditions,

then an increase in density to reach the HDH regime for higher P_{nbi} would be understandable. Finally, since these plasmas are generally collisional, i.e. in the Pfirsch-Schlüter regime, it is feasible that classical ‘temperature screening’ may explain the rapid decrease in τ_{imp} when HDH with its flat n_e -profiles is realized [31]. Thus, HDH is a two-stage process – first, flat n_e -profiles have to be established, which for H^+ leads to a jump in τ_E – and then as a result of the profile shape, temperature screening expels impurities from the core, thereby establishing a radiating edge. For NC (also collisional) the peaked n_e -gradients overcome any temperature screening effect and provoke central accumulation. Indeed, observations regarding reversal of iron accumulation with increasing \bar{n}_e on LHD have been tied to entering the $v^* > 1$ regime [32]. Finally, the preliminary finding on W7-AS that high density $\text{H}^0 \rightarrow \text{He}^{++}$ plasmas are plagued by impurity accumulation, even with flat n_e -profiles, is also a tendency predicted by classical theory.

Recapitulating, a new NBI-heated confinement regime – with some H-mode-like properties – has been established which develops beyond a critical density and can be maintained for at least 50 energy confinement times (mostly limited by the NBI availability). It exits over a wide variety of magnetic field configurations: $\tau_a = 5/8, 5/9$ and $5/10$ – with a large variation in distances between the separatrix and target plate δx , including limiter-bounded plasmas. HDH is achievable at power levels $P_{\text{nbi}} \sim 1\text{--}3.5$ MW (corresponding to absorbed power densities of $\sim 1.2\text{--}4$ MW/m³ averaged over the plasma volume) – for both co- and counter-injection – and a wide range of magnetic fields (0.9–2.5 T, not discussed). The density profiles are flat, with a steep gradient near the plasma edge, and show high separatrix densities (important for detachment). Energy confinement is in excess of τ_E^{ISS95} over the entire \bar{n}_e -range. Impurity confinement is poor, related to reduction of the inwards pinch velocity (or equivalently, just the effect of temperature screening?) with τ_{imp} approaching τ_E at the highest densities. The impurity radiation profiles are hollow, with edge radiation levels up to $\sim 50\%$ of P_{abs} yielding little degradation of τ_E , and up to 90% with acceptable deleterious effects on τ_E . A notable aspect of this confinement regime is its quiescent quasi-stationary state even close to operational boundaries, i.e. $P_{\text{rad}}/P_{\text{abs}}$ up to 90%, or $\langle \beta \rangle$ to 3.1% [33]. A clear isotope effect between deuterium and hydrogen is documented, but not yet understood. Now, with the cessation of W7-AS operation, it remains to explore in detail these various effects and possibilities with regard to the nature of HDH. To this end a massive database assembled since the beginning of divertor operation in April 2001 is available.

From the standpoint of divertor physics, the HDH regime has delivered the edge conditions necessary for comprehensive corroboration of the EMC3/EIRENE

code over the entire spectrum of relevant divertor conditions. Major facets of many experimental observations can already be understood, including the necessity of $E \times B$ drifts to explain certain up-down asymmetries. But the validation process has only just begun. The long-term outcome has the potential to deliver typical transport coefficients for W7-AS – thereby establishing the first elements of a size scaling in combination with W7-X or LHD – and to provide an established vehicle for the design and operational understanding of three-dimensional divertors.

References

- [1] H. Renner, Nucl. Fusion 40 (2000) 1083.
- [2] K. McCormick et al., Phys. Rev. Lett. 89 (July) (2002) 015001.
- [3] Y. Feng et al., J. Nucl. Mater. 266–269 (1999) 812.
- [4] K. McCormick et al., Plasma Phys. Control. Fusion 41 (1999) B285.
- [5] P. Grigull et al., Plasma Phys. Control. Fusion 43 (2001) A175.
- [6] P. Grigull et al., these Proceedings. PII: S0022-3115(02)01499-X.
- [7] U. Wenzel et al., these Proceedings. PII: S0022-3115(02)01545-3.
- [8] Y. Feng et al., these Proceedings. PII: S0022-3115(02)01463-0.
- [9] K. McCormick et al., in: Proceedings of the 12th and 13th International Stellarator Workshops, Madison 1999 and Canberra 2002, respectively.
- [10] K. McCormick et al., J. Nucl. Mater. 290–293 (2001) 920.
- [11] U. Stroth et al., Nucl. Fusion 36 (1996) 1063.
- [12] R. Burhenn et al., Europhys. Conf. Abst. 19c (Part III) (1995) 145, 21a (Part IV) (1997) 1609.
- [13] L. Giannone et al., Plasma Phys. Control. Fusion 42 (2000) 603.
- [14] R. Jaenicke et al., Plasma Phys. Control. Fusion 44 (2002) B193.
- [15] M. Hirsch et al., Plasma Phys. Control. Fusion 42 (2000) A231.
- [16] P. Grigull et al., J. Nucl. Mater. 290–293 (2001) 1009.
- [17] K. McCormick et al., Europhys. Conf. Abst. 25A (2001) 2097.
- [18] T. Hayashi et al., Phys. Fluids B 2 (1990) 392.
- [19] J. Geiger, T. Hayashi, in: Proceedings of the 29th EPS, Montreux, 2002, Europhys. Conf. Abst. 26B, P5.035.
- [20] R. Burhenn et al., Europhys. Conf. Abst. 24b (2000) 1000.
- [21] J.E. Rice et al., Phys. Plasmas 4 (1997) 1605.
- [22] J.P.T. Koponen et al., Nucl. Fusion 40 (2000) 365.
- [23] Y. Feng et al., Plasma Phys. Control. Fusion 44 (2002) 611.
- [24] N. Ramasubramanian et al., in: Proceedings of the 29th EPS conference, Montreux, 2002, Europhys. Conf. Abst. 26B, P5.034.
- [25] M. Greenwald et al., Phys. Plasmas 6 (1999) 1943; M. Greenwald et al., Plasma Phys. Control. Fusion 42 (2000) A263; J.A. Snipes et al., Plasma Phys. Control. Fusion 43 (2001) L23.

- [26] A. Hubbard et al., *Phys. Plasmas* 8 (2001) 2033.
- [27] E. Holzhauser, private communication.
- [28] S. Bäümel, private communication.
- [29] D.A. Mossessian et al., *Plasma Phys. Control. Fusion* 44 (2002) 423.
- [30] J.W. Hughes et al., *Phys. Plasmas* 9 (2002) 3019.
- [31] Yu. Igitkhanov et al., in: *Proceedings of the 29th EPS Conference, Montreux, 2002*, *Europhys. Conf. Abst.* 26B, P1.106.
- [32] Y. Nakamura et al., *Europhys. Conf. Abst.* 25A (2001) 1481.
- [33] A. Weller et al., in: *Proceedings of the 13th International Stellarator Conference, Canberra, 2002*.